# A Nulling Coronagraph for TPF-C

**B. M. Levine[1], M. Shao[1], R. Samuele[2], J.K. Wallace[1], S. Rao[1], R. Lyon[3], E. Schmidtlin[1], S.F. Fregoso[1], and F. Aguayo[1]**

## INTRODUCTION

This summary outlines a concept study for a high contrast instrument for the Terrestrial Planet Finder Coronagraph (TPF-C) mission (Levine 2006, Shao 2006). The objectives are to develop a nulling coronagraph based imager and spectrometer concept that will increase the number of planets TPF-C detects, and will expand the wavelength range of the spectrometer into the near-IR to enable detection of additional unique visible biomarkers. This instrument utilizes an alternative starlight suppression system (SSS) based on the principles of nulling interferometry, which allows inner working angles (IWA) within 2–3 $\lambda/D$ to be obtained, and also to measure low resolution (R=80) spectra. Equally important, this concept contains a post starlight suppression wavefront sensor (or calibration wavefront sensor) to increase the achievable contrast level, and to substantially decrease stability requirements during integration. The search for planets will be conducted at short wavelengths, where the IWA is smaller. Extending spectroscopy to 1.7µm, the visible and near infra-red signatures of likely atmospheric constituents include oxygen, ozone, water, methane, and carbon dioxide, some combinations of which are considered to be biosignatures. Coverage of the 0.5 ~1.7 µm wavelength range is done in intervals of 25% bandwidth. Our latest experimental results show null depths using white light that are within an order of magnitude of the required value.

## NULLING CONCEPT AND ARCHITECURE

The functional subsystems of a nulling coronagraph are shown in Figure 1. In this architecture, nuller #1 produces the deep null necessary to cancel the starlight. It passes this output to nuller #2, which broadens the angular extent of the null of starlight out to $\theta^4$, and transmits the rejected starlight to the Calibration Wavefront sensor for further processing. After nuller #2, any remaining starlight is caused by scattering from imperfections in the nuller optics. The fiber array then filters the high spatial frequency errors that may cause speckles in the same field of view as the planet. A part of the light from the fiber array goes to the science camera (or spectrophotometer), and the remainder of the light is mixed coherently in the Calibration Wavefront Sensor to provide an error signal to correct upstream phase errors and also to estimate residual starlight that can be subtracted on a post-detection basis.

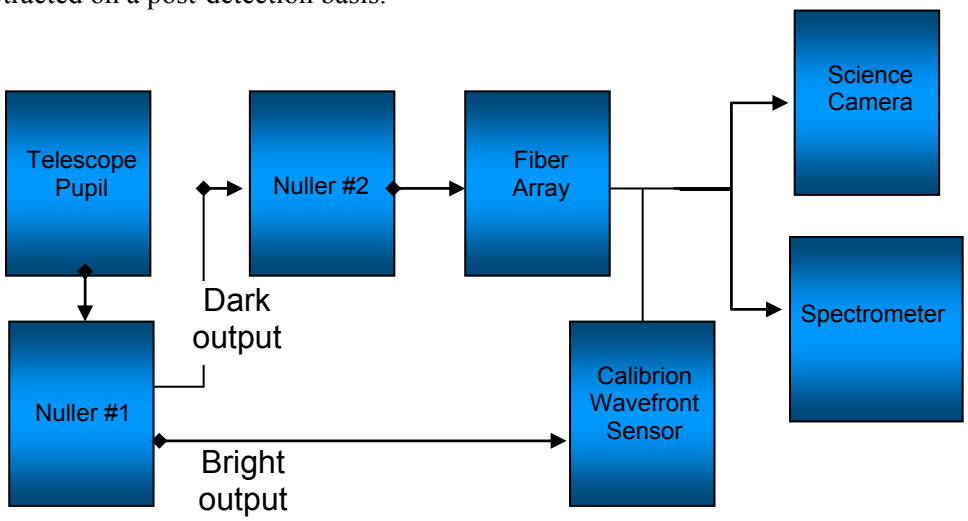


***Figure 1:*** *Top level architecture of a Nulling Coronagraph*

[1] Jet Propulsion Laboratory, California Institute of Technology
[2] Northrup Grumman Aerospace Systems
[3] NASA Goddard Space Flight Center

## USING A NULLING INTERFEROMETER INSTRUMENT WITH A SINGLE APERTURE TELESCOPE

In principle, a nulling interferometer effectively projects an interference pattern on the sky over the star-planet system to be imaged (Figure 2). The baseline, s, sets the fringe spacing. They attenuate the starlight and have 100% transmission for planet light when the optical path from the planet is $\lambda/2$ different from the star. For a modest sized aperture, about D=1m, a Jupiter-like planet can be resolved by synthesizing an interferometer with a 30-cm baseline, and at D=8m, an Earth-like planet can be resolved with a 50 cm baseline at $\lambda$=500 μm wavelength.

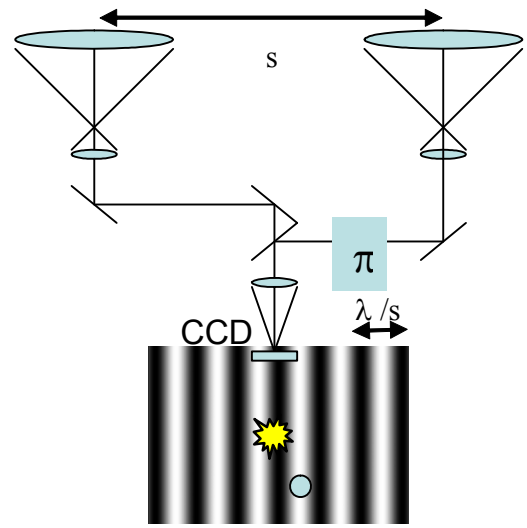


***Figure 2:*** *Imaging with nulling interferometry. A fringe pattern is superimposed over the star and planet to be imaged, the star is placed at the bottom of a deep, achromatic destructive (null) fringe, while planet on the constructive fringe is transmitted.*

The implementation for TPF-C calls for two nulling interferometers in a series. This arrangement synthesizes a four element nulling interferometer (the first nulling interferometer produces a deep null fringe pattern, and by directing its output into a second nulling interferometer, the null fringe becomes wider, and minimizes light leakage from the finite diameter of the star, and also from pointing errors). After nulling, an array of coherent single-mode optical fibers, coupled on both sides with (commercially available) lens arrays is used to filter the effects of any residual stellar leakage (scattering) due to imperfections in the telescope optics and optical train. A simple imaging system after this array forms the final extra-solar planet image.

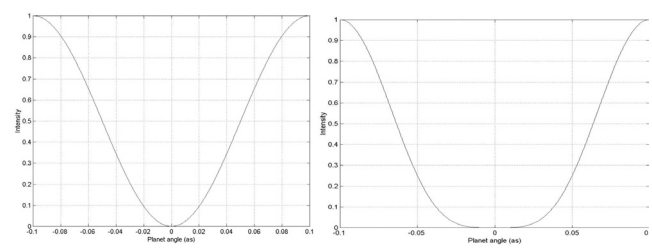

***Figure 3:*** *Intensity response of a 2 and a 4 element nulling inteterferometer. Left, fringe pattern over a 0.1 as field of view. Right, nulling depth over same field but with a 4 element nuller*

To introduce an achromatic π-radian phase shift in a different fashion, we use pairs of dielectric plates of differing thicknesses. Solutions for achromatic π-radian phase shifts (to the needed accuracy) exist with two glasses (Figure 4, lower right). Thus, for this experiment, the final layout for the beam combiner consists of identical two-glass pairs of (rotatable) dielectric phase retarders in each leg of the interferometer. Note that with the combination of common BK7 and Fused Silica optical glasses the theoretical minimum of $10^{-7}$ can be realized over a 25% bandwidth. (Morgan 2001)

Another advantage of the nulling coronagraph architecture is the single mode fiber array component to provide the deep null required, and also to relax the optical figure quality requirements of the primary telescope optics. With this array of fibers, wavefront errors at high spatial frequency, on a spatial scale smaller than any deformable mirror (DM) actuator, will be filtered out by the single-mode fibers instead of propagating to the science focal plane. If the optical fibers all have the same length (to $\lambda/20$) the planet light from each fiber combines to form a coherent off-axis image. The phase of the residual star light exiting the fiber array is random, hence it is scattered evenly across the whole field of view. In summary, wavefront errors on a spatial scale larger than the DM actuator spacing are corrected by active control of the DM and wavefront errors smaller than the actuator spacing are filtered out by the fiber array.

With an 8-m telescope, the airy pattern of the telescope has dropped ~$10^{-4}$ by the 5th airy ring, where we expect to find an earth at 10 pc. We need to suppress this by an additional factor of one million to achieve imaging. To keep scattered light below this $10^{-6}$ level, the optical system would need to be near-perfect (or have a Strehl ratio

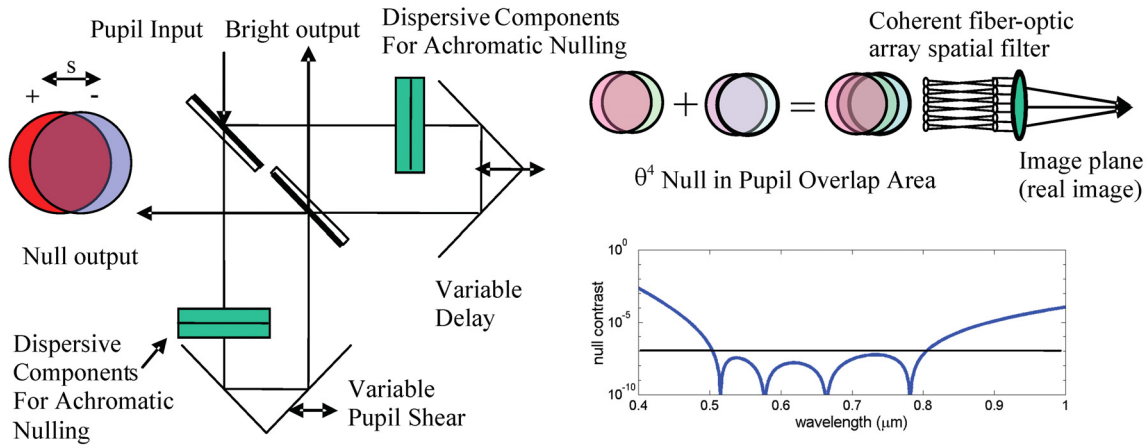


***Figure 4:*** *Visible nulling coronagraph instrument concept. Left, a concept for single-input symmetric nulling interferometer. Note that the two pupils emerge from the null output displaced (or sheared) by a distance, s, proportional to the baseline of the instrument. Lower right, Calculation of "pseudo-achromatic" null using two dielectric plates. Upper right, the major components of nulling coronagraph. By coupling two nulling interferometers, a 4 pupil overlap results in an interference fringe pattern proportional to $\lambda^4$. The fiber-optic array is a coherent spatial filter to reject residual scattered light. An imaging system then projects the pupil into the far-field to form an image.*

of 99.9999%), or the scattered light due to any minute optical figure imperfections results in a residual diffraction pattern from a conventional Lyot coronagraph. A Strehl of $10^{-6}$, in turn implies a full aperture optical figure that is almost perfect: ~λ/6000 rms, or ~1Å, hence the need for extreme wavefront control and Angstrom accuracy deformable mirrors. In our nulling coronagraph architecture, we plan to have a fiber array of approximately 1,000 fibers (arranged in an hexagonal array with a diameter of 39 fibers). Light from an 8m/39~ 20cm part of the primary falls on a lenslet which focuses the light into a single-mode fiber. At the output, this light is recollimated. Optically coupled to each fiber is a segmented deformable mirror in one arm of each nulling interferometer. This DM is used to control the amplitude and phase of the light. At the fiber input, if the starlight is suppressed by $10^{-7}$, then at the output a total of $10^{-7}$ of the starlight will appear as scattered light. Because in general the nulling process will produce residual leaked light with random phase, this $10^{-7}$ starlight will be scattered uniformly over the airy spot output field of view, with an average scattered light level of $10^{-10}$/airy spot.

## CALIBRATION SYSTEM

Although starlight is suppressed to $10^{-10}$, the resulting speckle pattern needs to be subtracted to a much lower level, $2 \times 10^{-11}$ for a 5 sigma detection of a planet. The post-starlight suppression system (SSS) sensor has two functions. One is to provide real-time feedback to the adaptive optics (AO) system to correct the state of scattered light, and to make the wavefront more perfect. The second function is to provide post-detection information on the amplitude and phase of this post-SSS wavefront in order to generate an estimate of the post-coronagraph point spread function (PSF) for subsequent correction by software subtraction.

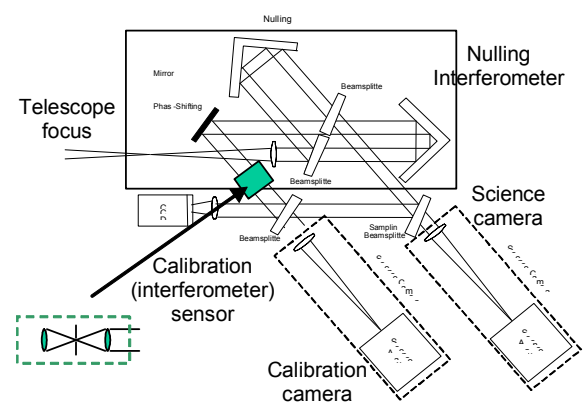


***Figure 5:*** *Concept for a calibration wavefront sensor with a nullling coronagraph.*

The default TPF procedure for subtracting residual starlight is to roll the telescope around the line of sight after about 2–4 hours of integration. For this method to work, the null has to be stable to $2 \times 10^{-11}$ for hours, which means that the wavefront must be stable to single digit picometers.

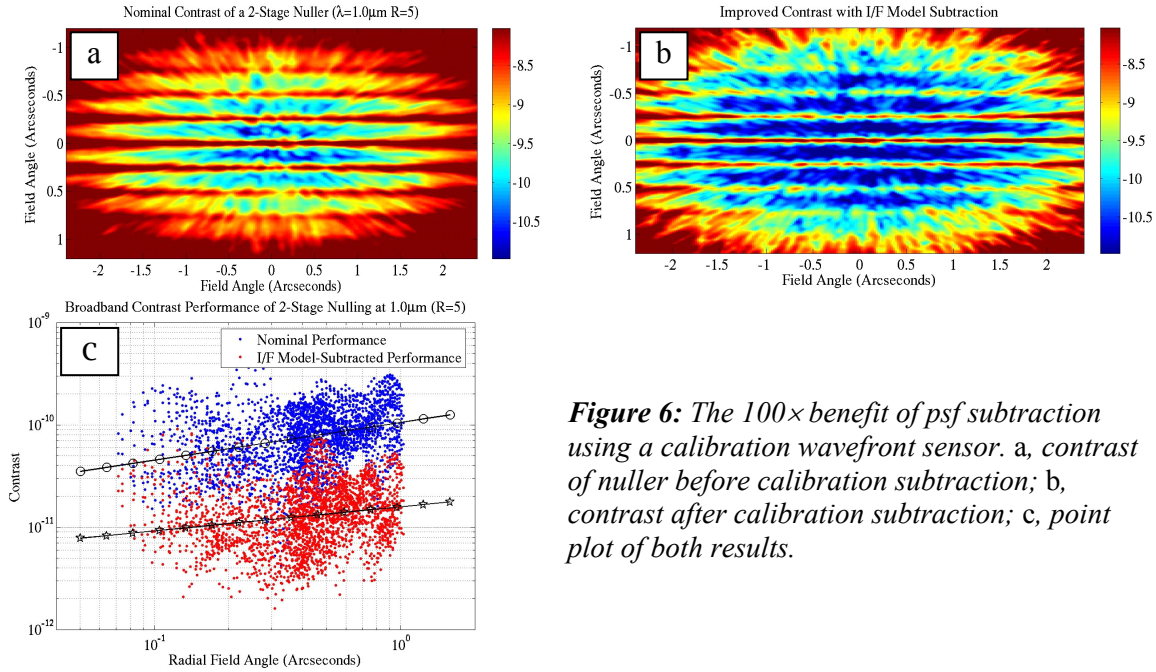


***Figure 6:*** *The 100× benefit of psf subtraction using a calibration wavefront sensor.* a*, contrast of nuller before calibration subtraction;* b*, contrast after calibration subtraction;* c*, point plot of both results.*

With a calibration interferometer, we measure the residual wavefront concurrent during science integration. Having both the image and an estimate of the wavefront error, the wavefront stability requirements can be relaxed by 4 to 6 orders of magnitude (picometer (pm) level stability over hours of integration versus pm stability over a fraction of a second). Wavefront changes caused by nanometer motions of the telescope secondary with respect to the primary mirror generate errors (focus, astigmatism, coma, etc.) that result in scattered light at 2-3-4 λ/D. Making any coronagraph/nuller work at small λ/D is difficult, but the calibration wavefront sensor makes 2 λ/D coronagraphs feasible.

The basic idea of the post starlight suppression system (SSS) wavefront sensor is to use the light blocked by the SSS as a "reference" beam in an interferometer to measure the post SSS electric field, both amplitude and phase. It comprises two beams: a reference beam and an unknown. The reference beam is created from the light that passes from the bright output of the first nulling interferometer. The light that forms the second (unknown) part is the nulled light picked off after the fiber array and before the science camera. The two beams are combined in the calibration camera, and using modulation with a 4-bin algorithm, the amplitude and phase of the stellar leakage is computed. The leakage point spread function is estimated by propagating this field into the far-field.

The calibration procedure produces a two-order-of-magnitude reduction of the speckle pattern as shown in the following simulation of the 8 m × 3.5 m TPF telescope (Fig. 6). The upper and lower figure shows the contrast level in the image before and after removal of the residual starlight psf. The point plot shows the individual contrast of each field point—somewhat like a contrast histogram with field angle.

## STATUS OF KEY EXPERIMENTS

Recent results from our nulling interferometer testbed yield contrast ratios at the $1.05 \times 10^{-6}$ level, with a 15% visible bandpass, which is equivalent to $10^{-9}$per airy spot. This result is at 65% of our final bandpass requirement, although limitations of our current configuration make major hardware changes essential to broadening the bandpass. We make the argument that broadening the bandpass should not necessarily adversely affect the null depth until beyond the 20% visible light level. Using the same setup we are able to reach monochromatic null depths of $1.11 \times 10^{-7}$ ($\lambda$ = 638 nm) averaged over three seconds (Samuele, 2007). This section describes our experimental approach for achieving deep broadband nulls, as well as error considerations and limitations, and the most recent results for our nulling coronagraph testbed.

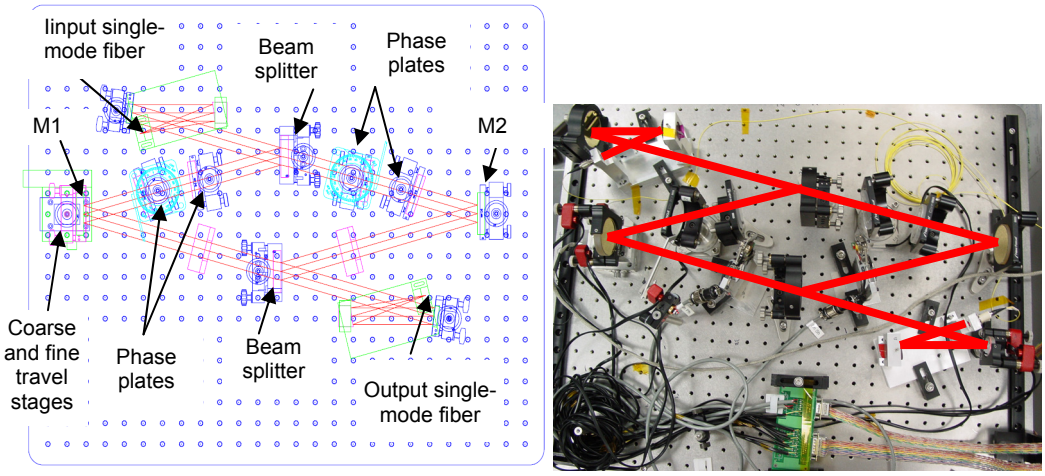


***Figure 7:*** *Nulling Test bed set up.*

The nulling interferometery experiment at JPL employs a modified Mach-Zehnder design. Maintaining a high degree of symmetry is necessary for deep nulling, so a meticulous approach is needed for both construction and alignment. The nuller core is composed of two bare-gold coated mirrors, one in each arm, and two highly symmetric, dielectrically-coated, beampslitters. The core mirrors and beamsplitters are aligned such that their coated surfaces are parallel to an arcminute--to mitigate pupil rotation (to be discussed later). The optics of the nuller are 50mm- in diameter, with each arm extending for roughly 650mm of path length.

To minimize path length fluctuations due to vibration, the nuller is positioned on three tiers of isolation. The testbed breadboard is directly mounted on visco-elastic, sorbothane bumpers internal to the vacuum chamber. Sorbothane is a material specifically designed for vibration dampening. Furthermore, the vacuum chamber itself is mounted on larger, weight-bearing sorbothane pucks. The vacuum chamber is then positioned on a 24 inch-thick Newport optical table, which is supported by pneumatic vibration-isolating legs. The whole lot is then positioned on a vibration-isolating pad. The interferometer is placed inside of a vacuum chamber—to mitigate the affects of atmospheric turbulence. However, we do not evacuate the chamber since we are able to achieve the required stability at atmosphere. We coarsely tune each glass type using interference fringes as a thickness metric. We also balance the deconstructive fringes directly adjacent to the central null, in order to achieve a symmetric white light interferogram. We finely tune our dispersion by using null depth as a direct metric. The upshot is that there is a panoply of solutions for differential glass thickness, and properly tuning the differential thickness with our rotation stage resolution is in fact feasible. The particular solution we use for our differential glass thicknesses are 481µm of Fused Silica and 393µm of BK7

## NULLING ERROR ANALYSIS

Each error term can be treated as an independent contributor to the overall null degradation. We use empirically determined values to estimate each error term's contribution, which linearly sum to yield our expected experimental null depth. We then check our experimental null result against that of the total null. This allows us to characterize the state of our interferometer's performance, and to evaluate which errors are contributing the lion's share. Table 1 shows a summary of the individual error terms.

An error assessment of our nulling interferometer includes the following measurable quantities: pupil rotation, birefringence, intensity mismatch, optical path fluctuations, and dispersion. Where pupil rotation, birefringence, and dispersion can be considered static errors, and intensity mismatch and optical path fluctuations dynamic errors Pupil rotation is purely geometrical and time-independent. It is caused by slight, out-of-plane folds that deviate from the parallelism of the mirror's surfaces. The end result is polarization leakage from one perpendicular state to another at the point of recombination. The first concern is getting the mirror surfaces parallel to within an arcminute. We accomplish this using a Fizeau interferometer to reflect off of each mirror's surface. We also place a mask at the interferometer input, at measure the relative offset induced by each interferometric arm.

***Table 1.*** *Nulling Interferometer Error Budget*

| Error Term | Equation | Variable | Empirical Value | Null Limit | % Contribution (broadband) |
|---|---|---|---|---|---|
| Pupil rotation | $N_{Pr} = \Theta^2/4$ | $\Theta$ | 0.01 deg | $7.6\times10^{-9}$ | 5.8 |
| Birefringence | $N_{Opd} = (2\pi\ \Delta OPD_{pol}/\lambda)^2/4$ | $\Delta OPD_{pol}$ | 0.04 nm | $9.7\times10^{-9}$ | 7.4 |
| Intensity mismatch | $N_{Im} = \Delta I^2/4$ | $\Delta I$ | 0.009% (laser)<br>0.03% (broadband*) | $2.25\times10^{-10}$<br>$2.3\times10^{-8}$ | 17.0 |
| Optical path fluctuations | $N_{Opd} = (2\pi\ \Delta OPD/\lambda)^2/4$ | $\Delta OPD$ | 0.06 nm rms | $8.7\times10^{-8}$ | 66.1 |
| Dispersion | $N_D = (2\pi\ \Delta OPD_\lambda/\lambda)^2/4$ | $\Delta OPD_\lambda$ | 0.014 nm | $4.9\times10^{-9}$ | 3.7 |
| Laser null (638 nm) | $N = N_{Pr} + N_B + N_{Im} + N_{Opd}$ | - | - | $1.05\times10^{-7}$ | - |
| Broadband null limit (15% WL) | $N = N_{Pr} + N_B + N_{Im} + N_{Opd} + N_D$ | - | - | $1.3\times10^{-7}$ | - |

We can adjust the beamsplitters to ensure a zero shear constraint. These two approaches allow us to tune and measure the pupil rotation to better than 0.01 degrees, and using the equation from Table 1, we estimate a null limit of $7.6 \times 10^{-9}$.

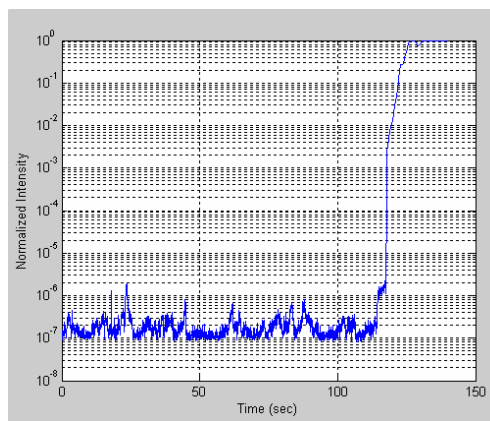


***Figure 8:*** *This data set shows our laser nulling result (638 nm) of $1.25 \times 10^{-7}$ averaged over 10 seconds, or $1.11 \times 10^{-7}$ averaged over 3 seconds. Null depths of roughly 8 and 9 million to one respectively. The first 120 seconds of data are at the deconstructive null, while the constructive peak follows.*

Birefringence is another time-independent error, by which polarization phase delay occurs when overly stressed regions of a transmissive optic, such as a beamsplitter, cause anisotropic regions in the substrate. Improper beamsplitters mounting, namely those mounts that use a setscrew, can significantly limit our null depth. We use a Malus' Law setup (i.e., two cross polarizers with the sample between them and a large area photodetector) to test for stress-induced biregrince. It is a strikingly clear affect that can be witnessed visually. To mitigate birefringence in our beamsplitters and dispersion plates we either use a spring loaded mounting mechanism or simply glue the optic to the mount. In this manner, we have managed to reduce the polarization phase delay to 0.04 nm or a null limit of $9.7\times10^{-9}$. We use null depth as a direct metric to evaluate polarization effects.

We used two edge filters, one with throughput longward of 590 nm and one with throughput shortward of 710 nm, to achieve a 15% white light bandpass profile, as shown in Figure 9. Broadband nulling with our 15% white light source, has yielded nulls as deep as $1.06 \times 10^{-6}$ averaged over a 3-second span, of which, the experimental results can be seen in Figure 6. The error analysis for each term is shown in Table 2.

Dispersion is still the dominant contributor to the lack of null depth. Experimentally this was seen as a lack of precision in the adjustment of the dispersion plates. As shown in Figure 10, the deepest null depth can be achieved over a range of differential thickness between the two dispersion plates, and when both plates can be tuned with infinite precision. The same curve is plotted on the right hand side of the figure given the step size resolution in our experiment. By replacing one of the glasses with a finer resolution stepping device, we should be able to achieve the required result.

## ACKNOWLEDGEMENTS

We wish to acknowledge the contributions of a number of engineers and scientists who made contributions to this effort prior to the start of this current TPF instrument concept study. R Bartos for mechanical engineering support and Dr. J. Green for simulations of wavelength dependent effects.

***Table 2.*** *Error analysis for the white light nulling experiment.*

| Source Null | Pupil Rotation | Intensity Mismatch | OPD Fluctuations | Birefringence | Dispersion |
|---|---|---|---|---|---|
| *Value achieved* | 0.01 Deg | 0.1% | 0.1 nm, rms | 0.04 nm | 0.15 nm |
| *Contribution to Null* | 7.62E-9 | 2.5E-7 | 2.42E-7 | 9.70E-9 | 4.89E-9 |
| *Net Null:* | 1.06E-6 (950K:1) | | | | |
| *% Contribution* | 1% | 24% | 23% | 1% | 51% |

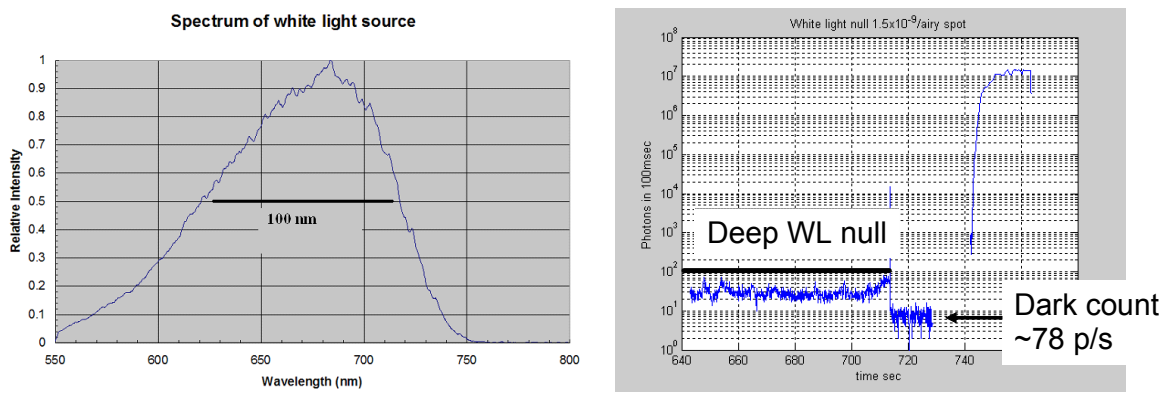


***Figure 9:*** *(Left) The 15% white light spectrum after propagation through one arm of the interferometer. The full width at half maximum is 100 nm. (Right) The resulting null plot showing nearly 1M:1 contrast (1.06 × $10^{-6}$)*

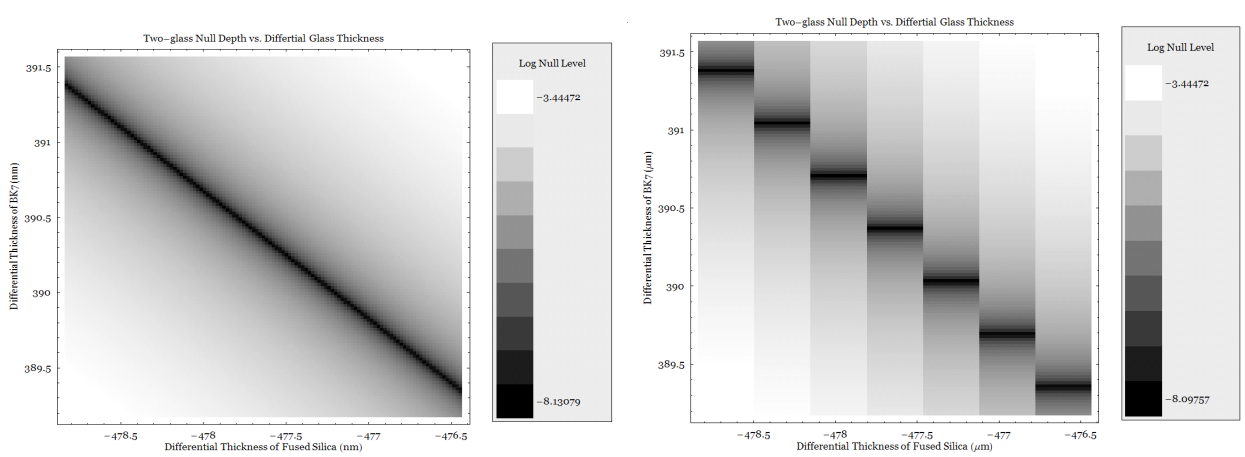


***Figure 10:*** *Finding the optimum differential spacing in a two glass null. (Left) null depth surface for the 2 glass null. (Right), Same null depth but using the step resolution limits in our experimental equipment. At any large "step" in one glass, the corresponding optimum null can be found with same device with sufficient resolution.*

## REFERENCES

Morgan, R. Ph.D., (2001), Thesis, University of Arizona. Optical Sciences.

Levine, B.M., et al., (2006), "The Visible Nulling Coronagraph—Architecture Definition and Technology Development," 207th Meeting of the AAS, Washington, DC.

Levine, B. M., et al, (2006), Proceedings of the SPIE, Volume 6265, pp. 62651A.

Shao, M., PI, (2006), "TPF-C Instrument Concept Study, Visible and Infrared Nulling Coronagraph Spectrometer," A Report Submitted to the Terrestrial Planet Finder Coronagraph Science and Technology Development Team, 7 March 2006, p4.

Samuele, R., et al., (2007), "Experimental Progress and Results of a Visible Nulling Coronagraph," IEEE Aerospace Conf. Paper #1366.